NASA Technical Memorandum 86730

Extraction of Aerodynamic Parameters for Aircraft at Extreme Flight Conditions

Kenneth W. Iliff

May 1985

National Aeronautics and
Space Administration

NASA Technical Memorandum 86730

Extraction of Aerodynamic Parameters for Aircraft at Extreme Flight Conditions

Kenneth W. Iliff
Ames Research Center, Dryden Flight Research Facility, Edwards, California

1985

NASA
National Aeronautics and
Space Administration
Ames Research Center
Dryden Flight Research Facility
Edwards, California 93523

EXTRACTION OF AERODYNAMIC PARAMETERS FOR AIRCRAFT AT EXTREME FLIGHT CONDITIONS

Kenneth W. Iliff
Senior Staff Scientist
NASA Ames Research Center
Dryden Flight Research Facility
Edwards, California 93523
U.S.A.

SUMMARY

The maximum likelihood estimator has been used to extract stability and control derivatives from flight data for many years. Most of the literature on aircraft estimation concentrates on new developments and applications, assuming familiarity with basic concepts. This paper briefly discusses the maximum likelihood estimator and the aircraft equations of motion that the estimator uses. The current strength and limitations associated with obtaining flight-determined aerodynamic coefficients in extreme flight conditions is assessed. The importance of the careful combining of wind tunnel results (or calculations) and flight results and the thorough evaluation of the mathematical model is emphasized. The basic concepts of minimization and estimation are examined for a simple computed aircraft example, and the cost functions that are to be minimized during estimation are defined and discussed. Graphic representations of the cost functions are given to help illustrate the minimization process. Finally, the basic concepts are generalized, and estimation of stability and control derivatives from flight data is discussed.

1. INTRODUCTION

Currently, an important thrust in the aerodynamic community is to specify completely the aerodynamic mathematical model for an aircraft. The ultimate goal of this thrust is to obtain a complete understanding of the physical laws (phenomenology) governing all aspects affecting the behavior of the aircraft. Presently we fall short of this goal in all flight regimes, but we have a particularly long way to go in extreme flight regimes, such as transonic or high-angle-of-attack flight, which are typically dominated by separated flow. As much as possible, we rely on experience and analogies that can be drawn from better understood regimes, such as subsonic flight with attached flow. But even with this wealth of experience, we still progress very slowly to the complete understanding of aircraft being flown at extreme flight conditions in complex flow fields.

In traditional regimes of less complex flow fields, certain aspects of understanding a particular phenomenon can sometimes proceed in a simple fashion, more or less ignoring the results of those working in different but related disciplines. This is not the case for understanding the physical laws that determine the characteristics of flight dominated by complex separated flows. We must begin by postulating candidate mathematical models, then test these models with all the techniques available. In addition, new testing techniques must be developed when existing techniques are not capable of testing portions of the mathematical model. Currently, the techniques that can contribute to validating the mathematical model can be divided into three categories: wind tunnel testing, computational fluid dynamic analysis, and flight testing.

Wind tunnel testing, computational fluid dynamic analysis, and flight testing serve complementary roles (with some overlap) to the overall validation of the mathematical model. Each category can contribute in a unique way to the overall validation. Quite probably, validation will not be possible without contributions from each category. System identification and parameter estimation techniques are needed to analyze flight test data because forces and moments cannot be measured directly. These techniques are used to extract force and moment coefficients from the motions measured in flight.

This paper discusses ways in which analysis of flight data can contribute to the formulation and testing of the mathematical model. To date, no comprehensive flight results are available for extreme flight conditions. This paper is intended to inform nonflight specialists of the current state of flight data coefficient estimation. The references cited in the paper reflect a representative sampling of current flight results. The paper first points out some of the differences between the approaches used for the less complicated, traditional flow regimes, and the approaches used for extreme flight conditions in the separated flow regime. It discusses the interrelationship of the mathematical model, the wind tunnel, and computational fluid dynamic results, and how they can be used with flight results. Parameter estimation, which is the primary method of extracting estimated coefficients from flight data so that results can be used to assess the mathematical model, is described in detail. The description is intended to emphasize the characteristics (both strengths and weaknesses) of system identification and parameter estimation. The mathematics involved are avoided wherever possible.

2. SYMBOLS

A,B,C,D,G	system matrices	C_n	coefficient of yawing moment
b	reference span, ft	c	reference chord, ft
C_ℓ	coefficient of rolling moment	$f(\cdot)$, $g(\cdot)$	general functions
C_m	coefficient of pitching moment	GG*	measurement noise covariance matrix

I_x, I_{xz}, I_y, I_z	moment of inertia about subscripted axis, slug-ft^2
i	general index
J	cost function
L	rolling moment divided by I_x, deg/sec^2
L'	rolling moment, ft/lb
m	mass, slug
N	number of time points or cases
n	state noise vector or number of unknowns
p	roll rate, deg/sec
q	pitch rate, deg/sec
$\bar{q}$	dynamic pressure, lb/ft^2
r	yaw rate, deg/sec
s	reference area, ft^2
T	time increment, sec
t	time, sec
u	control input vector
V	forward velocity, ft/sec
x	state vector
z	observation vector
$\tilde{z}_\xi$	predicted Kalman-filtered estimate
α	angle of attack, deg
β	angle of sideslip, deg
Δ	time sample interval, sec
δ	control deflection, deg
δ_a	aileron deflection, deg
η	measurement noise vector
μ	mean
ξ	vector of unknowns
σ	standard deviation
τ	time, sec
ϕ	bank angle, deg
ψ	heading angle, deg
∇_ξ	gradient with respect to ξ

Subscripts:

e	engine
m	measured quantity
$p,r,\alpha,\beta,\dot{\beta},\delta,\delta_a$	partial derivative with respect to subscripted quantity
0	bias or at time zero

Other nomenclature:

$\tilde{}$	predicted estimate
$\hat{}$	estimate
*	transpose
'	moment, ft-lb

3. PARAMETER ESTIMATION AT EXTREME FLIGHT CONDITIONS

General overviews of the problems of understanding aerodynamics and flight characteristics are given in Refs. 1 and 2. The issues affecting parameter estimation of flight characteristics and some of the results are given in Refs. 3 to 5. References 3 and 4 concentrate on estimation of characteristics obtained in traditional flight regimes not dominated by unsteady aerodynamics.

To appreciate the complexities of validating the mathematical model for flight data obtained at extreme flight conditions (such as high-angle-of-attack flight, transonic flight, or flight dominated by separated flow), it is useful to compare it to validation in traditional flight regimes, such as low angle of attack, subsonic, well established supersonic, or regimes with all flow essentially attached. The flow chart in Fig. 1 depicts the general elements required to validate the mathematical model in traditional flight regimes. Wind tunnel test and computational fluid dynamic calculations are used to design an aircraft with characteristics that meet the design criteria for a specific aircraft. These data are used along with information from other disciplines (such as control, structural, thermal, or propulsion characteristics) to define an aircraft. Once the aircraft is built, it will be flight tested. The data acquisition system must be specified based on the type of aircraft and the flight regimes to be flown. The mathematical model expressed by equations of motion, which is representative of the aircraft dynamic characteristics (usually including stability and control derivatives), is then specified. Representative forms of the equations of motion are given in Refs. 6 to 8. Then, knowing the mathematical model and the flight conditions of interest, the pertinent mass characteristics are estimated. At this point, the maneuvers that are needed for model validation are defined and flown. A parameter estimation technique, such as a maximum likelihood estimator, is then used to determine the stability and control derivative estimates from the flight data (Refs. 9 to 11). (Parameter estimation is discussed in detail in a later section.) These parameter estimates are assessed, summarized, and compared to the best predicted set of computational and wind tunnel estimates. These predicted estimates may be the data set that was used to design the aircraft, or they may be that data supplemented with subsequent computational and wind tunnel results produced after the aircraft design was frozen. The comparison of flight estimates with other estimates may generate additional flight, computational, or wind tunnel tests. These estimates can then

be assessed in the same way, as depicted by the flow chart. When all tests are complete and their results compared, a composite representation of these tests is put in a data base. This data base may be used to aid in future design or may be put into a real-time simulator to be used for pilot training, control system redesign, or mission analysis.

In contrast to Fig. 1, Fig. 2 shows the additional complexity involved in the mathematical model validation for data obtained at extreme flight conditions. Figure 2 represents only the crosshatched area from Fig. 1. The two figures are to about the same level of detail. Figure 2 is representative of the process and is not necessarily an exact representation of the procedure followed by any given analyst. The flow chart of figure 2 not only has more elements, but also is significantly more complex in that the "flow" between the various elements may need to be iterated more times. In the following sections, each of the various elements is discussed in detail.

3.1 MATHEMATICAL MODEL SELECTION

Since the primary outcome of the flow chart is the validation of the mathematical model, it is appropriate to specify the mathematical model first. Initially, a mathematical model or a set of candidate mathematical models must be specified. It should be kept in mind that each element of the chart is subject to change as the entire flow chart is iterated. The form of the model may be specified by wind tunnel tests, as shown in Fig. 2. Probably the most promising set of mathematical models based on strong phenomenological consideration is given in Ref. 12. The models are derived under the assumptions that (1) response to a steady motion is itself steady, (2) the response is a single-valued function of the orientation of the body (although it may be nonlinear), and (3) the responses are linear in the motion rates. The authors of Ref. 12 showed how a nonlinear variation of the responses with coning rate could be accommodated. The models as given do not include the effects of control deflection. Control terms can be added to the model in a fashion analogous to the way that the flow angle (α and β) terms are included, and probably would initially be functions of angle of sideslip and angle of attack. Reference 12 also discusses the inclusion of terms that involve aerodynamic hysteresis. For the mathematical model to have much generality, it would probably need to account for hysteresis as it is highly probable that hysteresis occurs at extreme flight conditions. However, regardless of the initial model chosen, if the subsequent analysis shows a need for hysteresis terms, they can be added during a future iteration. It is highly probable that for the gyrations observed at extreme flight conditions, terms involving nonlinear coning effects and aerodynamic hysteresis would need to be included in the general mathematical model. Reference 13 discusses how phenomena that violate the restrictions of Ref. 12 can be accommodated within the mathematical model.

3.2 MASS CHARACTERISTICS

The next element of Fig. 2 is the specification of the mass characteristics. These characteristics have, in the past, been given very little consideration in the analysis of data obtained at extreme flight conditions, because experience gained in the analysis of data obtained in traditional flight regimes has shown that the data only need to be known to an accuracy of about 10 percent. If an error of 10 percent in mass characteristics is present in the analysis of traditional flight data, it will probably be noted when comparing flight results to wind tunnel estimates, and, if necessary, can be compensated for at that point. However, data obtained at an extreme flight condition is usually highly oscillatory in all axes, and the kinematic cross-coupling effects are highly dependent on the mass characteristics. The mass is usually easily determined, but the moments of inertia are difficult to determine accurately. Any error in accounting for the kinematic coupling terms becomes an error that is added to the remaining terms or the aerodynamic terms.

The following equations (also given in Refs. 6 to 8) demonstrate this difficulty:

$$\dot{p}I_x - \dot{r}I_{xz} - qr(I_y - I_z) - pqI_{xz} = \bar{q}sbC_\ell \tag{1}$$

$$\dot{q}I_y - rp(I_z - I_x) - (r^2 - p^2)I_{xz} - NrI_{x_e} = \bar{q}scC_m \tag{2}$$

$$\dot{r}I_z - \dot{p}I_{xz} - pq(I_x - I_y) + qrI_{xz} + NqI_{x_e} = \bar{q}sbC_n \tag{3}$$

Equations (1) to (3) assume that I_{xy} and I_{yz} are zero. The individual kinematic terms (left side of the equations) are frequently larger than the aerodynamic terms during wild gyrations and spins. Even C_m is affected by I_x, I_y, I_z, I_{xz}, and I_{x_e} in a nonlinear fashion. This is still true when the rates are known exactly. I_x, I_y, and I_z are always significant terms, and I_{xz} usually is. I_{x_e} would affect any aircraft with a rotating engine. A current challenge is to obtain an accurate set of these moments of inertia to within less than 1 percent, which may not be within the current state of the art.

It should also be noted that these numbers vary significantly with the amount and location of the fuel during the maneuver. Since many of the maneuvers of interest result in wild gyrations, an additional source of error is fuel sloshing. The issues involving fuel quantity and fuel location (sloshing or otherwise) and the rotating engine mass make unpowered aircraft more attractive as initial candidates for assessing mathematical models.

Current experience shows that if very detailed calculations are made for the weight, location, and inertias of each component (no matter how small) of an aircraft, then fairly consistent values of the mass characteristics are obtained. The other method of obtaining moments of inertia is by swinging the vehicle,

as discussed in Ref. 14. The author's experience has shown that moments of inertia obtained by swinging a vehicle are adequate for the traditional regimes if done with extreme care. These experimentally obtained numbers are in good agreement with calculated numbers when both are done with extreme care. In general, it seems doubtful that swinging the vehicle will provide adequate accuracy for analysis of an aircraft during wild gyrations.

3.3 MANEUVER DEFINITION

Definition of the maneuvers to be flown is the next element of the flow chart. Certain characteristic motions are necessary to assess any given mathematical model. Reference 12 discusses the characteristic motions required to assess the models it proposes. These characteristic motions can be generated, at least in theory, in a wind tunnel by using a specific rig, such as the rotary rig (Ref. 15). Unfortunately, an aircraft always flies close to the trimmed condition, even when undergoing violent gyrations. The time required for a vehicle to complete a wild gyration, including a spin, is very short; therefore, these motions provide very little information because all the state variables are changing rapidly. Figure 3 shows an example of this for an aircraft entering a spin. In addition, oscillations tend to repeat a set of state variable values each oscillation. All these problems result in trajectories that repeat, are highly transient, and contain only a small amount of information about the desired characteristic motion. Therefore, no matter how carefully a maneuver to be flown is specified, one has very little control over how much of the characteristic motion is obtained. This is not to say that one cannot obtain useful information from careful specification of maneuvers; it simply means that the "matrix" of test conditions is limited compared to those that can be obtained in the wind tunnel. Although this is an obvious contribution of wind tunnel testing (a highly controlled experiment), flight test data do have the advantage of giving exactly the correct motions throughout the flight envelope, regardless of what the assumed mathematical model is. Even though the aircraft cannot give specific characteristic motions, it does give a great deal of highly dynamic motion that can result in invaluable information when analyzed with modern parameter estimation techniques. This information describes the aircraft motion along the flight trajectory, but it does not completely define the global mathematical model.

One would assume that aerodynamic characteristics (information about the "true" mathematical model) can be obtained from the combined applicaton of computational, wind tunnel, and flight data analysis techniques that cannot be determined from any single technique.

3.4 INSTRUMENTATION REASSESSMENT

The next element in the flow chart of Fig. 2 is the reassessment of instrumentation. When an aircraft is flying at an extreme flight condition, the accurate measurement of the flow (flow angles, and dynamic and static pressure) can be greatly compromised because of separated or vortical flows, or shock waves in the vicinity of the instrument or sensor. The sensor will normally measure only the local flow, which may or may not be representative of the free-stream flow. In a highly dynamic gyration, the flow measurement is likely to be better at one time than it is at another. This suggests that flow measurements should be made at several locations so that the true free-stream flow can be inferred from the combination of measurements. If a fixed pitot head is used when flying at a high angle of attack, the pitot head should be canted to obtain accurate pressures at high angle of attack. Flow angles can be measured with either vanes or pressure sensors. Problems can occur with either of these techniques because of the dynamic characteristics of the vane or the time lags in the pressure sensors. A detailed discussion of flow measurements is beyond the scope of this paper, but it is nonetheless extremely important to obtain accurate measurements of the flow. It may seem that the free-stream flow conditions could be obtained from inertial measurements. This would be true if one could fly in an airmass that does not move with respect to the inertial frame of reference. One might occasionally encounter a portion of the airmass that is at rest, but the rule is that the airmass is constantly in motion. The motion exhibited by winds and turbulence not only varies spatially but also varies as a function of time. This makes it imperative to obtain external flow measurements if one is to make sense of flight data obtained at extreme conditions. Perfect flow measurements cannot be made by any intrusive sensor; therefore, one must be able to improve the raw flow measurements by some means. The next section treats this problem.

3.5 DATA AND TRAJECTORY RECONSTRUCTION

The next element in the flow chart of Fig. 2 is data and trajectory reconstruction, which is sometimes referred to as consistency checking. This is the generic procedure that is intended to improve the raw flow measurements. Reconstruction can improve all the measurements in that reconstruction procedures force the data to conform to the physical laws of a rigid aircraft. They also reduce the sensor modelling errors and the sensor measurement noise. Most of these procedures use the extended Kalman filter as the basic algorithm. The extended Kalman filter provides a very powerful and consistent technique to improve the aircraft data measurements, but the procedure can be very time consuming because weighting factors must be determined for each of the measurements. The relative weighting of one measurement to another is representative of the confidence one has in a given measurement. This confidence can be a function of vehicle attitude or flow condition, so in most cases it will vary over time and from maneuver to maneuver. Another difficulty encountered in using the extended Kalman filter is that the filter implementation may become unstable, forcing the analyst to use *ad hoc* procedures to stabilize the filter. A complete discussion of data and trajectory reconstruction techniques is beyond the scope of this paper, but a representative sample of these techniques is given in Refs. 11, 16, and 17.

During the data and trajectory reconstruction phase, measurements obtained from the ground can be used in conjunction with those obtained on board the aircraft. Figure 2 shows these ground sources as radar and optical measurements. The primary source of optical data is phototheodolite. In the near future, data from the Global Positioning System (GPS) will also be available. Radar, optical, and GPS sources are independent, inertially based data sources that can be used to improve the accuracy of the reconstructed trajectory. It should be pointed out that data and trajectory reconstruction techniques are also used for

data obtained in the traditional flight regimes. These techniques are used to improve onboard measurements and reduce the measurement noise so that noise-sensitive regression or equation error techniques can be used. These techniques are discussed thoroughly in Ref. 11.

3.6 MODEL STRUCTURE DETERMINATION

The key element of Fig. 2 is the model structure determination (MSD) element. As shown, it is strongly coupled with other major elements of the flow chart. The model structure referred to here is simply another way of stating the form of the mathematical model. The proposed mathematical models of Ref. 12 are model structures. The concept of this block is slightly more restrictive in that there may be a large collection of candidate elements in the mathematical model or model structure. Model structure determination is the procedure that, by some criterion, selects for the model structure only those terms that can be accurately estimated from the available flight data. Of course, the model structure can also be specified by information from computation, wind tunnel, or previous flights. However, the intent of the MSD element is to further define the model structure based on the information content of the flight data. That is, the candidate elements of the model structure could be some of those proposed in Ref. 12. Some elements could be eliminated, or their values fixed, on the basis of wind tunnel tests, such as rotary balance tests. The candidate elements can be based purely on phenomenological considerations or they can be based purely on *ad hoc* considerations.

Most of the MSD algorithms use stepwise regression to assess the effect of individual elements on the motion observed from a flight maneuver. Some of the proposed MSD algorithms are described in Refs. 7, 18, and 19. The details of the algorithm are not described here, but a heuristic description is given. The algorithm is a regression technique in which the individual candidate elements of the proposed mathematical model are evaluated one by one. The elements are rejected if they have a low correlation with acceleration terms or a high correlation based on a given set of flight data to one of the other more significant elements. Being rejected indicates that the element makes no significant contribution to explaining the behavior of the flight data. The stepwise regression technique can be automated to select the best set of elements from a given maneuver. Independent testing on other data is needed to determine the final set of elements of the mathematical model. The models that stepwise regression algorithms evaluate frequently use spline formulations with variable knot partitions (break points). This means that the data are partitioned as a function of the more important aircraft variables, such as angle of attack or elevator deflection. The stepwise regression algorithm can select the types of candidate elements, including the spline, as well as the partitions for the flight data.

3.7 RESULT EVALUATION

The next step of Fig. 2 compares the output of the MSD algorithm for several maneuvers and looks for consistency or inconsistency in the elements being selected. The types of errors that are consistent for several maneuvers are also examined. The outcome of this step is either (1) that the proposed mathematical model is in all likelihood a good model and we should proceed to the final analysis of the flight data, or (2) that the model is found lacking and additional elements are required. At this point, the flight results are compared with the computational and special apparatus wind tunnel results. Inconsistencies in this comparison may indicate that further modifications to the mathematical model or additional computational or wind tunnel results are required.

This concludes the discussion of Fig. 2 and how it iterates to converge on a promising mathematical model before final maximum likelihood estimation analysis is performed. The details of the maximum likelihood estimation are given in the next section. Some of the more encouraging results for analysis of flight data at extreme flight conditions are given in Refs. 5 to 7, and 20 to 25.

In summary, the simplest mathematical model is selected based on physical laws. The types of wind tunnel apparatuses and tests required are determined based on this model. The results of the tests may indicate the need for changes in the mathematical model (to make it either less or more complex). Accurate values of the mass characteristics must be obtained as a function of fuel loading. Aircraft maneuvers must be defined to stimulate the characteristic motions defined by the mathematical model. The best instrumentation possible for obtaining data at extreme flight conditions must be defined and installed. Data and trajectory reconstruction must be performed to improve the flow measurements, to reduce the sensor noise and modelling errors, and to include radar and optical data if available. The simplest model structure for a given set of data must be determined. This can be done with stepwise regression techniques since the "measurement" noise was reduced in the preceeding step. Elements and coefficient values from the wind tunnel tests may be used in this step. The consistency between the mathematical model and data for several maneuvers must be evaluated at this point. If the model is found lacking, the mathematical model may need to be reevaluated and additional computations or wind tunnel tests may need to be performed. If either of these is necessary, the steps in the flow chart are iterated again to reevaluate the flight data. If the model is found adequate, we proceed to the final analysis with the maximum likelihood estimator. The model may still be found inadequate at this point, indicating the need for a refinement in the mathematical model. Once the model is refined, the flowchart steps are interated again.

4. SIMPLE EXAMPLE OF PARAMETER ESTIMATION

In the previous section the overall procedures were discussed for extracting aerodynamic information from flight data. That discussion contrasted the relative complexities for analyzing data obtained at traditional flight conditions with the analysis of data obtained at extreme flight conditions. A parameter estimation phase is required for either of these regimes. Parameter estimation techniques are necessary because direct force and moment measurement is not possible for an aircraft in flight. These techniques extract aerodynamic coefficents from aircraft flight motions. The parameter estimation phase is essentially the same for data obtained in either of these flight regimes. The differences are in (1) the complexity of the underlying mathematical model that has been assumed, (2) the difficulty in getting the

parameter estimation algorithm to converge, and (3) the interpretation of the results. All of these differences pertain to the degree to which the concepts of parameter estimation are involved and not whether or not the concept is fundamental to the estimation. Therefore, the remainder of the paper illustrates the concepts involved in applying the parameter estimation algorithms to flight data. The parameter estimation concepts are illustrated with simple models, but the concepts generalize to include the most complex analysis of data from extreme flight regimes.

The parameter estimation algorithm discussed here is the maximum likelihood estimation algorithm, or output error method. The theory and formulation of the method are given in Ref. 26, and an example of the computer code used for this type of analysis is given in Refs. 9 and 10. The mathematical models used in these examples are the same as those used for analysis in the traditional linear flight regimes for estimating stability and control coefficients. The same estimation algorithm is used whether the mathematical model formulation is linear or nonlinear.

The models of Ref. 12, including the one that accounts for aerodynamic hysteresis, can be implemented and the algorithm will remain essentially unchanged. In essence, the model must be written in some functional form. The functional form can be in a piecewise linear or spline form. Increasing the complexity of the model does not change the essential estimation algorithm, it just increases the complexity of the implementation and the time required to execute the computer codes. In general, models that are highly nonlinear, include a very complicated structure, or have a large number of states will require larger and more complex flight maneuvers to provide satisfactory estimates from any estimation algorithm. Computer roundoff errors are the only real limitations on how complex the model (written in functional form) can be or how many unknown aerodynamic coefficients can be determined from high-quality flight maneuvers.

4.1 DESCRIPTION OF A PARAMETER ESTIMATION PROGRAM

The Iliff-Maine code (MMLE3 program) described in Ref. 9 is used throughout the remainder of this paper to obtain estimates of the coefficients of the differential equations of motion.

Figure 4 illustrates the maximum likelihood estimation concept for aircraft data as used by MMLE3. The measured response of the aircraft is compared with the estimated response, and the difference between these responses is called the response error. The Gauss-Newton computational algorithm (Ref. 26, section (2.5.2)) is used to find the coefficient values that maximize the likelihood functional. Each iteration of this algorithm provides new estimates of the unknown coefficients on the basis of the response error. These new estimates of the coefficients are then used to update the mathematical model of the aircraft, providing a new estimated response and, therefore, a new response error. The updating of the mathematical model continues iteratively until a convergence criterion is satisfied. The estimates resulting from this procedure are the maximum likelihood estimates.

The maximum likelihood estimator also provides a measure of the reliability of each estimate based on the information obtained from each dynamic maneuver. This measure of the reliability, analogous to the standard deviation, is called the Cramèr-Rao bound (Ref. 25) or the uncertainty level. The Cramèr-Rao bound as computed by current programs should generally be used as a measure of relative accuracy rather than absolute accuracy. The bound is obtained from the approximation of the information matrix (Ref. 26).

4.2 EQUATIONS FOR SIMPLE EXAMPLE

The basic concepts involved in a parameter estimation problem can be illustrated by using a simple example representative of a realistic aircraft problem. The example chosen here is representative of an aircraft that exhibits pure rolling motion from an aileron input. This example, although simplified, typifies the motion exhibited by many aircraft in particular flight regimes, such as the F-14 aircraft flying at high dynamic pressure, the F-111 aircraft at moderate speeds with the wing in the forward position, and the T-37 aircraft at low speed. The model of this example is linear, but the results from a more complex example would lead to the same conclusions. A more complex example only makes the basic concepts more difficult to illustrate.

Derivation of an equation describing this motion is straightforward. Figure 5 shows a sketch of an aircraft with the x-axis perpendicular to the plane of the figure (positive forward on the aircraft). The rolling moment (L'), roll rate (p), and aileron deflection (δ_a) are positive as shown. For this example, the only state is p and the only control is δ_a. The result of summing moments is

$$I_x\dot{p} = L'(p,\delta_a) \tag{4}$$

The first-order Taylor expansion then becomes

$$\dot{p} = L_p p + L_{\delta_a}\delta_a \tag{5}$$

where

$$L' = I_x L$$

Since the aileron is the only control, it is notationally simpler to use δ instead of δ_a for the discussion of this example. Equation 5 can then be written as

$$\dot{p} = L_p p + L_\delta \delta \tag{6}$$

In the nondimensional form this becomes

$$\dot{p}I_x = \bar{q}sb\left(C_{\ell_p}\frac{pb}{2V} + C_{\ell_\delta}\delta\right) \tag{7}$$

The dimensional form of Eq. (6) is used hereafter since it is simpler notationally.

Equation (6) is a simple aircraft equation where the forcing function is provided by the aileron and the damping by the damping-in-roll term, L_p. Equation (7) can be written and solved in the same form as Eq. (65) of Ref. 12, but the addition of the hysteresis term in Eq. (65) would only complicate the essential character of the estimation. In subsequent sections we examine in detail the parameter estimation problem where Eq. (6) describes the system. For this single-degree-of-freedom problem, the maximum likelihood estimator is used to estimate either L_p or L_δ or both for a given computed time history.

Now that we have specified the equations describing our simple model, we can examine the characteristics of the maximum likelihood estimation in this simple case. Chapters 2, 7, and 8 of Ref. 26 describe maximum likelihood estimation in detail for the general case. Our simple example requires only a few of the results from that reference, so those results are repeated briefly below.

Where, as in our example, there is no state noise and the equations of motion are linear, the equations are

$$x(t_0) = x_0 \tag{8}$$

$$\dot{x}(t) = Ax(t) + Bu(t) \tag{9}$$

$$z(t_i) = Cx(t_i) + Du(t_i) + Gn_i \tag{10}$$

where x is the state vector, z is the observation vector, and u is the control vector.

The maximum likelihood estimator minimizes the cost function

$$J(\xi) = \frac{1}{2}\sum_{i=1}^{N}[z(t_i) - \tilde{z}_\xi(t_i)]^*(GG^*)^{-1}[z(t_i) - \tilde{z}_\xi(t_i)] \tag{11}$$

where GG^* is the measurement noise covariance, and $\tilde{z}_\xi(t_i)$ is the computed response estimate of z at t_i for a given value of the unknown parameter vector ξ. The cost function is a function of the difference between the measured and computed time histories.

To minimize the cost function $J(\xi)$, we can apply the Newton-Raphson algorithm which chooses successive estimates of the vector of unknown coefficients, $\hat{\xi}$. Let L be the iteration number. The L + 1 estimate of $\hat{\xi}$ is then obtained from the L estimate as follows:

$$\hat{\xi}_{L+1} = \hat{\xi}_L - \left[\nabla^2_\xi J(\hat{\xi}_L)\right]^{-1}\left[\nabla^*_\xi J(\hat{\xi}_L)\right] \tag{12}$$

The first gradient is defined as

$$\nabla_\xi J(\xi) = -\sum_{i=1}^{N}[z(t_i) - \tilde{z}_\xi(t_i)]^*(GG^*)^{-1}[\nabla_\xi \tilde{z}_\xi(t_i)] \tag{13}$$

The Gauss-Newton approximation to the second gradient is

$$\nabla^2_\xi J(\xi) \cong \sum_{i=1}^{N}[\nabla_\xi \tilde{z}_\xi(t_i)]^*(GG^*)^{-1}[\nabla_\xi \tilde{z}_\xi(t_i)] \tag{14}$$

The Gauss-Newton approximation, which is sometimes referred to as modified Newton-Raphson, is computationally much easier than Newton's method because the second gradient of the innovation never needs to be calculated. In addition, it can have the advantage of speeding the convergence of the algorithm.

Equation (11) then gives the cost function for maximum likelihood estimation. The weighting GG^* is unimportant for this problem, so let it equal 1. For our example, Eqs. (9) and (10) become $x_i = p_i$ and $z_i = x_i$. Therefore, Eq. (11) becomes

$$J(L_p,L_\delta) = \frac{1}{2}\sum_{i=1}^{N}[p_i - \tilde{p}_i(L_p,L_\delta)]^2 \tag{15}$$

where p_i is the value of the measured response p at time t_i and $\tilde{p}_i(L_p,L_\delta)$ is the computed time history of $\tilde{p}$ at time t_i for $L_p = \hat{L}_p$ and $L_\delta = \hat{L}_\delta$. Throughout the rest of the paper, where simulated data are used, the measured time history (simulated) refers to p_i, and the computed time history refers to $\tilde{p}_i(L_p,L_\delta)$.

The computed time history is a function of the current estimates of L_p and L_δ, but the measured time history is not. The expression for obtaining $\tilde{p}_i(L_p,L_\delta)$ is given in Ref. 9.

The maximum likelihood estimate is obtained by minimizing Eq. (11). The Gauss-Newton method described earlier is used for this minimization. Equation (12) is used to determine successive values of the estimates of the unknowns during the minimization. The first and second gradients are defined by Eqs. (13) and (14). For this simple problem, $\hat{\xi} = [\hat{L}_p \ \hat{L}_\delta]^*$ and successive estimates of L_p and L_δ are determined by updating Eq. (12).

The entire procedure can now be written for obtaining the maximum likelihood estimates for this simple example. To start the algorithm, initial estimates of L_p and L_δ are needed. This is the value selected for $\hat{\xi}_0$. With Eq. (12), $\hat{\xi}_1$ and subsequently $\hat{\xi}_L$ are defined by using the first and second gradients of $J(L_p,L_\delta)$ from Eq. (15). The gradients for this particular example from Eqs. (13) and (14) are

$$\nabla_\xi J(\hat{\xi}_L) = -\sum_{i=1}^{N}(p_i - \tilde{p}_i)\nabla_\xi \tilde{p}_i \tag{16}$$

$$\nabla_\xi^2 J(\hat{\xi}_L) \cong \sum_{i=1}^{N}(\nabla_\xi \tilde{p}_i)^* \ (\nabla_\xi \tilde{p}_i) \tag{17}$$

With the specific equations defined in this section for this simple example, we can now proceed in the next section to the computational details of a specific example.

4.3 COMPUTATIONAL DETAILS OF MINIMIZATION

In the previous section we specified the equations for a simple example and described the procedure for obtaining estimates of the unknowns from a dynamic maneuver. In this section we give the computational details for obtaining the estimates. Some of the basic concepts of parameter estimation are best shown with computed data where the correct answers are known. Therefore, in this section we study two examples involving simulated time histories. The first example is based on data that have no measurement noise, which results in estimates that are the same as the correct value. The second example contains significant measurement noise similar to the noise that occurs in data obtained at extreme flight conditions; consequently, the estimates differ from the correct values. Throughout the rest of the paper, where simulated data are used, the term "no-noise case" is used for the case with no noise added and "noisy case" for the case where noise has been added.

For this simulated example, 10 time sample points are used. The simulated data, which we refer to as the measured data, are based on Eq. (6). We use the same correct values of L_p and L_δ (-0.2500 and 10.0, respectively) for both examples. In addition, the same input (δ) is used for both examples, the sample interval (Δ) is 0.2 sec, and the initial conditions are zero. Tables of all the significant intermediate values are given for each example. These values are given to four significant digits, although to obtain exactly the same values with a computer requires the use of 13 significant digits, as in the computation of these tables. In both examples, the initial values of L_p and L_δ (or $\hat{\xi}_0$) are -0.5 and 15.0, respectively. More complete detailed calculations are given in Ref. 8.

4.3.1 Example With No Measurement Noise

The measurement time history for no measurement noise (no-noise case) is shown in Fig. 6. The aileron input starts at zero, goes to a fixed value, and then returns to zero. The resulting roll-rate time history is also shown.

For each value of L (number of iterations), we can get ξ_L by using Eq. (12). Table 1 shows the values for $\hat{L}_p$, $\hat{L}_\delta$, and J for each iteration. In three iterations the algorithm converges to the correct values to four significant digits for both L_p and L_δ. $\hat{L}_\delta$ overshoots slightly on the first iteration and then comes quickly to the correct answer. $\hat{L}_p$ overshoots slightly on the second iteration.

Figure 7 shows the match between the measured data and the computed data for each of the first three iterations. The match is very good after two iterations. The match is nearly exact after three iterations.

Although the algorithm has converged to four-digit accuracy in L_p and L_δ, the value of the cost function, J, continues to decrease rapidly between iterations 3 and 4. This is a consequence of using the maximum likelihood estimator on data with no measurement noise. Theoretically, using infinite accuracy, the value of J at the minimum should be zero. However, with finite accuracy, the value of J becomes small but never quite zero. This value is a function of the number of significant digits being used. For the 13-digit accuracy used here, the cost eventually decreases to approximately 0.3×10^{-28}.

4.3.2 Example With Measurement Noise

The data used in the example with measurement noise (noisy case) are the same as those used in the previous section, except that pseudo-Gaussian noise has been added to the roll rate. The time history is shown in Fig. 8. The signal-to-noise ratio is quite low in this example, as one would expect in data obtained at extreme flight conditions. This is readily apparent when Figs. 6 and 8 are compared. Table 2

shows the values of $\hat{L}_p$, $\hat{L}_\delta$, and J for each iteration. The algorithm converges in four iterations. The behavior of the coefficients as they approach convergence is much like the no-noise case. The most notable result of this case is the converged values of $\hat{L}_p$ and $\hat{L}_\delta$, which are somewhat different from the correct values. The difference in converged values is caused by the measurement noise. As stated in Section 3.5, DATA AND TRAJECTORY RECONSTRUCTION, the parameter estimates can be improved by reducing the measurement noise. The match between the measured and computed time history is shown in Fig. 9 for each iteration. No change in the match is apparent for the last two iterations. The match is very good considering the low signal-to-noise ratio of this example.

In Fig. 10, the computed time history for the no-noise estimates of L_p and L_δ is compared to that for the noisy-case estimates of L_p and L_δ. Because the algorithm converged to values somewhat different than the correct values, the two computed time histories are similar but not identical.

4.4 COST FUNCTIONS

In the previous section, we obtained the maximum likelihood estimates for computed time histories by minimizing the values of the cost function. To fully understand what occurs in this minimization, we must study in more detail the form of the cost functions and some of their more important characteristics. In this section, the cost function for the no-noise case is discussed briefly. The cost function of the noisy case is then discussed in more detail. The same two time histories studied in the previous section are examined here. The noisy case is more interesting because it has a meaningful Cramèr-Rao bound and is more representative of aircraft flight data.

First we will look at the one-dimensional case, where L_δ is fixed at the correct value, because it is easier to grasp some of the characteristics of the cost function in one dimension. Then we will look at the two-dimensional case, where both L_p and L_δ are varying. It is important to remember that everything shown in this paper on cost functions is based on simulated time histories that are defined by Eq. (5). For every time history we might choose (computed or flight data), a complete cost function is defined. For the case of n variables, the cost function defines a hypersurface of n + 1 dimensions. It might occur to us that we could just construct this surface and look for the minimum, avoiding the need to bother with the minimization algorithm. However, this is not a reasonable approach because, in general, the number of variables is greater than two. Therefore, the cost function can be described mathematically but not pictured graphically.

4.4.1 One-Dimensional Case

To understand the many interesting aspects of cost functions, it is easiest to first look at cost functions having one variable. In an earlier section, the cost function of L_p and L_δ was minimized. That cost function is most interesting in the L_p direction. Therefore, the one-variable cost function studied here is $J(L_p)$. All discussions in this section are for $J(L_p)$ with L_δ equal to the correct value, 10. Figure 11 shows the cost function plotted as a function of L_p for the case where there is no measurement noise (no-noise case). As expected for this case, the minimum cost is zero and occurs at the correct value of L_p = -0.2500. It is apparent that the cost increases much more slowly for a more negative L_p than for a positive L_p. Physically this makes sense since the more negative values of L_p represent cases of high damping, and the positive L_p represents an unstable system. Therefore, the p_i for positive L_p becomes increasingly different from the measured time history for small positive increments in L_p.

In Fig. 12, the cost function based on the time history with measurement noise (noisy case) is plotted as a function of L_p. The correct value of L_p (-0.2500) and the value of L_p (-0.3218) at the minimum of the cost (3.335) are both indicated on the figure. The general shape of the cost function in Fig. 12 is similar to that shown in Fig. 11. Figure 13 shows the comparison between the cost functions based on the noisy and no-noise cases. The comments relating to the cost functions' dependence on L_p error in the no-noise case also apply to the cost function based on the noisy case. Figure 13 shows clearly that the two cost functions are shifted by the difference in the value of L_p at the minimum and increased by the difference in the minimum cost. The difference shown here illustrates the penalty if one does not pay close attention to reducing the measurement noise. A similar shift would occur if an incorrect model were used. This was discussed earlier in reference to data reconstruction.

Figure 14 shows the gradient of $J(L_p)$ plotted as a function of L_p for the noisy case. This is the function for which we were trying to find the zero (or equivalently, the minimum of the cost function) using the Gauss-Newton method that is discussed in a previous section. The gradient is zero at L_p = -0.3218, which corresponds to the value of the minimum of $J(L_p)$.

The usefulness of the Cramèr-Rao bound was discussed earlier. At this point it is useful to digress briefly to discuss some of the ramifications of the Cramèr-Rao bound for the one-dimensional case. The Cramèr-Rao bound has meaning only for the noisy case. In the noisy example, the estimate of L_p is -0.3218 and the Cramèr-Rao bound is 0.0579. This relatively large value of the Cramèr-Rao bound is caused by the low signal-to-noise ratio (data from extreme flight conditions) for this case. The Cramèr-Rao bound indicates that we are getting a poor estimate of the rate-dependent coefficient L_p. The Cramèr-Rao bound is an estimate of the standard deviation of the estimate. One would expect the scatter in the estimates of L_p to be of about the same magnitude as the estimate of the standard deviation. For the one-dimensional case discussed here, the range of L_p (-0.3218) plus or minus the Cramèr-Rao bound (0.0579) nearly includes the correct value of L_p (-0.2500). If noisy cases are generated for many time histories (adding different measurement noise to each time history), then the sample mean and sample standard

deviation of the estimates for these cases can be calculated. Table 3 gives the sample mean, sample standard deviation, and the standard deviation of the sample mean (standard deviation divided by the square root of the number of cases) for 5, 10, and 20 cases. The sample mean, as expected, gets closer to the correct value of -0.2500 as the number of cases increases. This is also reflected by the decreasing values column of Table 3, which are estimates of the error in the sample mean. The next to last column of Table 3 shows the sample standard deviations, which indicate the approximate accuracy of the individual estimates. This standard deviation, which stays more or less constant, is approximately equal to the Cramèr-Rao bound for the noisy case being studied here. In fact, the Cramèr-Rao bounds for each of the 20 noisy cases used here (not shown in the table) do not vary significantly from the values found for the noisy case being studied. Both of these results are in good agreement with the theoretical characteristics (Ref. 27) of the Cramèr-Rao bounds and maximum likelihood estimators in general.

The examples shown here indicate the value of obtaining more sample time histories (maneuvers). More samples improve confidence in the estimate of the unknowns. The same result holds true in analyzing actual flight time histories (maneuvers); thus it is always advisable to obtain several maneuvers at a given flight condition to improve the best estimate of each derivative. This is especially true when analyzing data obtained at extreme flight conditions.

The size of the Cramèr-Rao bounds and of the error between the correct value and the estimated value of L_p is determined to a large extent by the length of the time history and the amount of noise added to (or modeling error present in) the correct time history. For the example being studied here, it is apparent from Fig. 8 that the amount of noise being added to the time history is large. The effect of the power of the measurement noise (GG*, Eqs. (9) and (10)) on the estimate of L_p for the time history is given in Table 4. The estimate of L_p is much improved by decreasing the measurement noise power. A reduction in the value of G to one-tenth of the value in the noisy example being studied yields an acceptable estimate of L_p. For flight data, the measurement noise is reduced by improving the accuracy of the output of the measurement sensors or through data and trajectory reconstruction, as discussed in an earlier section.

4.4.2 Two-Dimensional Case

In this section, the cost function (dependent on both L_p and L_δ) is studied. The no-noise case is examined first, followed by the noisy case.

Even though the cost function is a function of only two unknowns, it becomes much more difficult to visualize than the one-unknown case. The cost function over a reasonable range of L_p and L_δ is shown in Fig. 15. The cost increases rapidly in the region of positive L_p and large values of L_δ. The reason is just an extension of the argument for positive L_p given in the previous section. The shape of the surface can be depicted in greater detail if we examine only the values of the cost function less than 200 for L_p less than 1.0. Figure 16 shows a view of this restricted surface from the upper end of the surface. The minimum must lie in the curving valley that gets broader as we go to the far side of the surface. Now that we have a picture of the surface, we can look at the isoclines of constant cost on the L_p-versus-L_δ plane. These isoclines are shown in Fig. 17. The minimum of the cost function is inside the closed isocline. The steepness of the cost function in the positive-L_p direction is once again apparent. Inside the closed isocline the shape is more nearly elliptical, indicating that the cost is nearly quadratic here, so fairly rapid convergence in this region would be expected. The L_p axis becomes an asymptote in cost as L_δ approaches zero. The cost is constant for $L_\delta = 0$ because no response would result from any aileron input. The estimated response is zero for all values of L_p, resulting in constant cost.

Figure 17 includes the minimum value of the cost function, which, as seen in the earlier example (Table 1), occurs at the correct values for L_p and L_δ of -0.2500 and 10.0, respectively. This is also evident from the cost function surface shown in Fig. 18. The surface has its minimum at the correct value. As expected, the value of the cost function at the minimum is zero.

Sometimes nonestimation specialists get the impression that the final estimate of a parameter (stability and control coefficient) is dependent on the starting value, but this is not the case for the maximum likelihood estimator. If the maximum likelihood estimator is used to obtain the maximum likelihood estimates, the estimate will be the minimum of the cost function, as shown in Figs. 13, 16, and 18. These minima are independent of the starting values. If the estimation technique includes *a priori* information in the cost function (such as a maximum *a posteriori* estimator), the minimum value is affected by *a priori* estimates of the coefficient. Usually the *a priori* value is used as the starting value for maximum likelihood estimators, leading some to the conclusion that the estimate is a function of the starting values for all estimators. For all cases that are discussed in this paper the minimum of the cost function is independent of the starting value. Of course, the further one starts the algorithm from the minimum value, the longer it takes the algorithm to converge. Therefore, especially for data obtained at extreme flight conditions, it is important to have good wind tunnel and computational fluid dynamic estimates. These other estimates also can prove useful for fixing values of coefficients of the estimates as we did L_δ in the one-dimensional case. This information can also be used in the maximum *a posteriori* estimators.

As shown before in the one-dimensional case, the primary difference between the cost functions for the no-noise and noisy cases was a shift in the cost function. In that instance, the noisy case was shifted so that the minimum was at a higher cost and a more negative value of L_p. In the two-dimensional case, the no-noise and noisy cost functions exhibit a similar shift. For two dimensions, the shift is in both the L_p and L_δ directions. The shift is small enough that the difference between the two cost functions is not visible at the scale shown in Fig. 15 or from the perspective of Fig. 16. Figure 19 shows the

isoclines of constant cost for the noisy case. The figure looks much like the isoclines for the no-noise case shown in Fig. 17. The difference between Figs. 17 and 19 is a shift in L_p of about 0.1. This is the difference in the value of L_p at the minimum for the no-noise and noisy cases. Heuristically, one can see that the same would be true for cases with more than two unknowns. The primary difference between the two cost functions is near the minimum.

The next logical part of the cost function to examine is near the minimum. Figure 20 shows the same view of the cost function for the noisy case as was shown in Fig. 10 for the no-noise case. The shape is roughly the same as that shown in Fig. 18, but the surface is shifted such that its minimum lies over $L_p = -0.3540$ and $L_\delta = 10.24$, and is shifted upward to a cost function value of approximately 3.3.

To get a more precise idea of the cost of the noisy case near the minimum, we once again need to examine the isoclines. The isoclines (Fig. 21) in this region are much more like ellipses than they are in Figs. 17 and 19. We can follow the path of the minimization example used before by including the results from Table 2 on Fig. 2. The first iteration ($L = 1$) brought the values of L_p and L_δ very close to the values at the minimum. The next iteration essentially selected the values at the minimum when viewed at this scale. One of the reasons the convergence is so rapid in this region is that the isoclines are nearly elliptical, indicating that the cost is very nearly quadratic in this region. Had we started the Gauss-Newton algorithm at a point where the isoclines are much less elliptical (as in some of the border regions in Fig. 19), the convergence would have been much slower initially, but much the same as it entered the nearly quadratic region of the cost function. The process, of course, results in the same minimum regardless of the starting values.

A final point to be made in examining cost functions deals with the relative shape of the cost function. Although these shapes are somewhat apparent in Figs. 15, 16, and 17, they are most readily studied for constant-cost isoclines as in Figs. 19 and 21. The result we want here is related to the steepness of the cost near the minimum. The minimum shown in Fig. 21 occurs at a cost of 3.3. If we project the isocline for the cost of $J = 5$ onto the L_p axis, we intersect values for L_p of approximately 0 and -0.7. This is a small increase in cost (about 50 percent), yet the values spanned for L_p are ±100 percent of the noise-contaminated estimate. If we project the same isocline onto the L_δ axis, we intersect values for L_δ of approximately 9 and 11. This is only a change of about 10 percent for the same increase in cost. This shows that the rate-dependent coefficient L_p has a much flatter shape near the minimum than does the control derivative L_δ, which means that relative accuracy in estimating L_p is much poorer than for L_δ. This result can be generalized for all the rate-dependent coefficients as compared with the primary stability and control coefficients, such as L_β, N_β, and L_δ. Going one step further, the cross and cross-coupling coefficients (such as L_r or $L_{\dot{\beta}}$) are even flatter near the minimum than are the rotary coefficients (such as L_p and N_r). This fact points out the necessity of obtaining the best possible estimates from other predictive techniques for rate-dependent coefficients. These coefficients can be estimated from rotary balance or forced oscillation tests. It remains to be seen if these wind tunnel estimates will be more accurate than the flight-determined estimates. Currently the thought is that each source of these coefficients will have deficiencies, but with information from both sources we may be able to determine the relative importance of accurate values of the coefficients in defining a good model. One final item on the relative flatness of the cost functions is that the flatness can be reduced by (1) increasing the length of the flight maneuver, (2) reducing the number of unknown coefficients (fixing the values at computed or wind tunnel values), (3) reducing the noise in the instrumentation system through better instruments or through data reconstruction, (4) reducing equation errors with better estimates of the mass characteristics, and (5) increasing the information content of the maneuver by defining and flying specifically designed maneuvers at extreme flight conditions.

Before concluding our examination of the two-dimensional case, we need to examine the Cramèr-Rao bound. Figure 22 shows the uncertainty ellipsoid, which is based on the Cramèr-Rao bounds defined in an earlier section. The relationships between the Cramèr-Rao bound and the uncertainty ellipsoid are discussed in Ref. 27. The uncertainty ellipsoid almost includes the correct value of L_p and L_δ. The Cramèr-Rao bound for L_p and L_δ can be determined from the projection of the uncertainty ellipsoid onto the L_p and L_δ axes, and compared with the values of the Cramér-Rao bound, which are 0.1593 and 1.116 for L_p and L_δ, respectively.

5. CONCLUDING REMARKS

This paper discusses the increased complexity and effort required in comparing parameter estimation in the traditional and extreme flight regimes. The analysis in the extreme flight regimes requires more care and understanding in selecting the mathematical model, the mass characteristics, the maneuvers flown, and the type and location of instrumentation sensors. Additional analytical techniques, such as data and trajectory reconstruction and model structure determination, are needed. The evaluation of results is also more complex, and several iterations may be required to evaluate the mathematical model. The essential characteristics of the maximum likelihood estimation technique are studied with the help of a simple, but representative, simulated aircraft flight example. The basics of minimization and the general concepts of cost functions are discussed. The example showed the value of low measurement noise, multiple estimates at a given flight condition, and the Cramèr-Rao bounds. The relative flatness of the cost functions in the direction of the rate-dependent coefficients is demonstrated. This flatness is shown to result in poor estimation of these coefficients. The need for a close interplay between computation, wind tunnel, and flight analysis is also discussed.

6. REFERENCES

1. Dynamic Stability Parameters. AGARD-CP-235, 1978.

2. Dynamic Stability Parameters. AGARD-LS-114, 1981.

3. Methods for Aircraft State and Parameter Identification. AGARD-CP-172, 1975.

4. Parameter Identification. AGARD-LS-104, 1979.

5. AIAA Atmospheric Flight Mechanics Conference Proceedings. AIAA CP849, Aug. 1984.

6. Iliff, Kenneth W.: Aircraft Identification Experience. AGARD-LS-104, paper 6, 1979.

7. Klein, Vladislav; Batterson, James G.; and Murphy, Patrick C.: Determination of Airplane Model Structure From Flight Data by Using Modified Stepwise Regression. NASA TP-1916, 1981.

8. Iliff, Kenneth W.; and Maine, Richard E.: Maximum Likelihood Estimation with Emphasis on Aircraft Flight Data. Proceedings of Workshop on Identification and Control of Flexible Space Structures, June 1984.

9. Maine, Richard E.; and Iliff, Kenneth W.: User's Manual for MMLE3, a General FORTRAN Program for Maximum Likelihood Parameter Estimation. NASA TP-1563, 1980.

10. Foster, G.W.: A Description of the Weighted Least Squares Output-Error Method of Parameter Identification. RAE TM FS 215, 1978.

11. Mulder, J.A.; Jonkers, H.L.; Horsten, J.J.; Breeman, J.H.; and Simons, J.L.: Analysis of Aircraft Performance, Stability and Control Measurements. Parameter Identification, AGARD-LS-104, paper 5, 1979.

12. Tobak, Murray; and Schiff, Lewis B.: Aerodynamic Mathematical Modeling — Basic Concepts. Dynamic Stability Parameters, AGARD-LS-114, paper 1, 1981.

13. Tobak, Murray; and Chapman, Gary T.: Nonlinear Problems in Flight Dynamics Involving Aerodynamic Bifurcations. Unsteady Aerodynamics — Fundamentals and Application of Aircraft Dynamics, AGARD paper 25, May 1985.

14. Wolowicz, Chester H.; and Yancy, Roxannah B.: Experimental Determination of Airplane Mass and Inertial Characteristics. NASA TR R-433, 1974.

15. Malcolm, Gerald N.; and Schiff, Lewis B.: Recent Developments in Rotary-Balance Testing of Fighter Aircraft Configurations at NASA Ames Research Center. Unsteady Aerodynamics — Fundamentals and Applications of Aircraft Dynamics, AGARD paper 18, May 1985.

16. Klein, V.; and Schies, J.R.: Compatability Check of Measured Aircraft Responses Using Kinematic Equations and Extended Kalman Filter. NASA TN D-8514, 1977.

17. Bach, R.E., Jr.; and Wingrove, R.C.: Applications of State Estimation in Aircraft Flight Data Analysis. AIAA-83-2087, 1983.

18. Gupta, N.K.; Hall, W.E., Jr.; and Trankle, T.L.: Advanced Methods of Model Structure Determination from Test Data. AIAA J. Guidance & Control, vol. 1, no. 3, 1978, pp. 197-204.

19. Trankle, T.L.; Vincent, J.H.; and Franklin, S.N.: System Identification of Nonlinear Aerodynamic Models. The Techniques and Technology of Nonlinear Filtering and Kalman Filtering, AGARD-AG-256 paper 7, 1982

20. Iliff, Kenneth W.; Maine, Richard E.; and Shafer, Mary F.: Subsonic Stability and Control Derivatives for an Unpowered, Remotely Piloted 3/8-Scale F-15 Airplane Model Obtained From Flight Test. NASA TN D-8136, 1976.

21. Klein, V; and Batterson, J.G.: Estimated Low-Speed Aerodynamic Parameters of an Advanced Fighter from Flight and Wind Tunnel Data. 14th ICAS Congress, Sept. 1984.

22. Anderson, L.C.; Vincent, J.H.; and Hildreth, B.L.: AV-8B System Identification Results from Full Scale Development Flight Test Program. AIAA-83-2746, AIAA/AHS/IES/SETP/SFTE/DGLR 2nd Flight Testing Conference, Las Vegas, Nev., U.S.A, Nov. 1983.

23. Iliff, K.W.: Stall/Spin Flight Results for the Remotely Piloted Spin Research Vehicle. AIAA Atmospheric Flight Mechanics Conference, AIAA-80-1563, Aug. 1980.

24. Gupta, Naren K.; and Iliff, Kenneth W.: Identification of Aerodynamic Indicial Functions Using Flight Data. AIAA Atmospheric Flight Mechanics Conference, AIAA-82-1375, Aug. 1982.

25. Ross, A.J.; and Edwards, G.F.: Correlation of Predicted and Free-Flight Responses Near Departure Conditions of a High Incidence Research Model. Unsteady Aerodynamics — Fundamentals and Applications to Aircraft Dynamics, AGARD paper 31, May 1985.

26. Maine, Richard E.; and Iliff, Kenneth W.: Identification of Dynamic Systems. AGARD Flight Test Techniques Series, AGARD-AG-300-vol.2, 1985.

27. Maine, Richard E.; and Iliff, Kenneth W.: The Theory and Practice of Estimating the Accuracy of Dynamic Flight-Determined Coefficients. NASA RP-1077, 1981.

Table 1 Pertinent values for no-noise case as a function of iteration

L	$\hat{L}_p(L)$	$\hat{L}_\delta(L)$	J_L
0	-0.5000	15.00	21.21
1	-0.3005	9.888	0.5191
2	-0.2475	9.996	5.083×10^{-4}
3	-0.2500	10.00	1.540×10^{-9}
4	-0.2500	10.00	1.060×10^{-14}

Table 2 Pertinent values for noisy case as a function of iteration

L	$\hat{L}_p(L)$	$\hat{L}_\delta(L)$	J_L
0	-0.5000	15.00	30.22
1	-0.3842	10.16	3.497
2	-0.3518	10.23	3.316
3	-0.3543	10.25	3.316
4	-0.3542	10.24	3.316
5	-0.3542	10.24	3.316

Table 3 Mean and standard deviations for estimates of L_p

Number of cases, N	Sample mean, $\mu(\hat{L}_p)$	Sample standard deviation, $\sigma(\hat{L}_p)$	Sample standard deviation of the mean, $\sigma(\hat{L}_p)/\sqrt{N}$
5	-0.2668	0.0739	0.0336
10	-0.2511	0.0620	0.0196
20	-0.2452	0.0578	0.0129

Table 4 Estimate of L_p and Cramèr-Rao bound as a function of the square root of noise power

Square root of noise power, G	Estimate of $\hat{L}$	Cramèr-Rao bound
0.0	-0.2500	-------
0.01	-0.2507	0.00054
0.05	-0.2535	0.00271
0.10	-0.2570	0.00543
0.2	-0.2641	0.0109
0.4	-0.2783	0.0220
0.8	-0.3071	0.0457
1.0	-0.3218	0.0579
2.0	-0.3975	0.1248
5.0	-0.6519	0.3980
10.0	-1.195	1.279

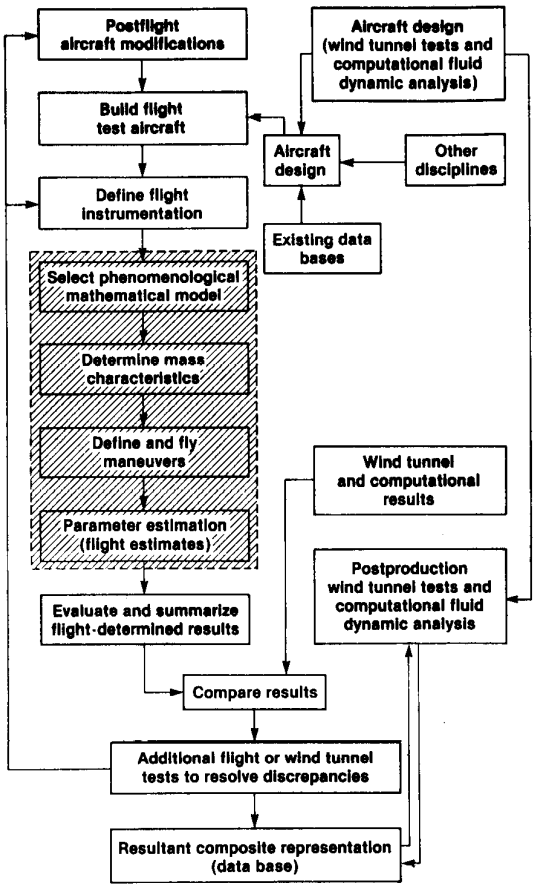

Fig. 1 Approach to validating mathematical model in traditional flight regimes.

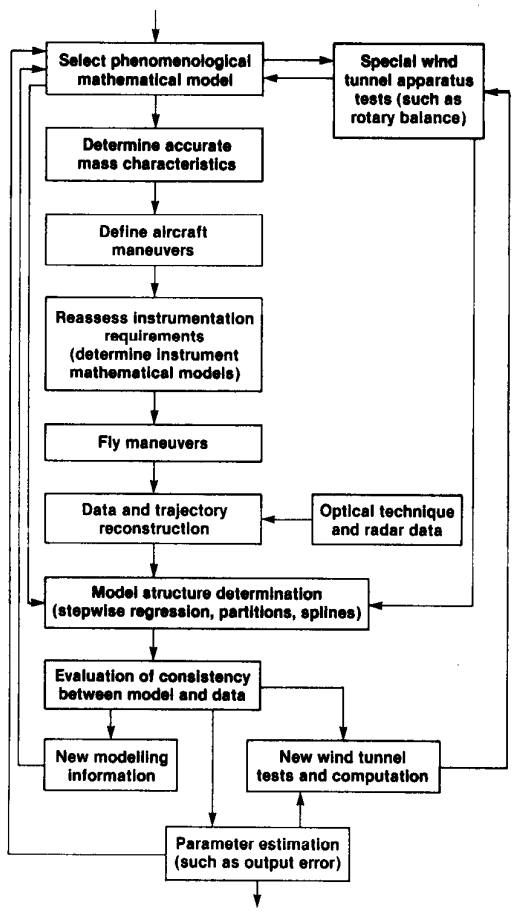

Fig. 2 Approach to validating mathematical model at extreme flight conditions.

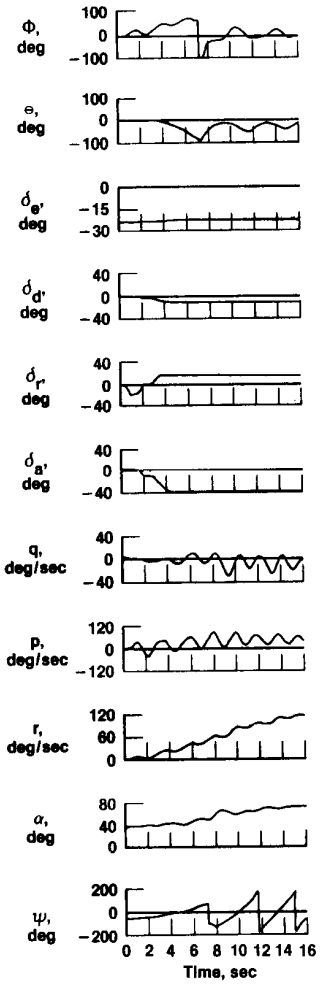

Fig. 3 Typical time history of spin entry.

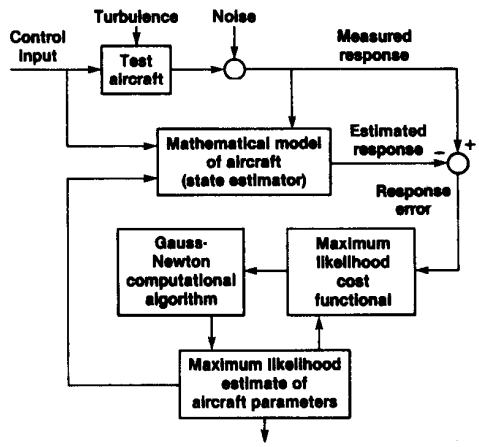

Fig. 4 Maximum likelihood estimation concept.

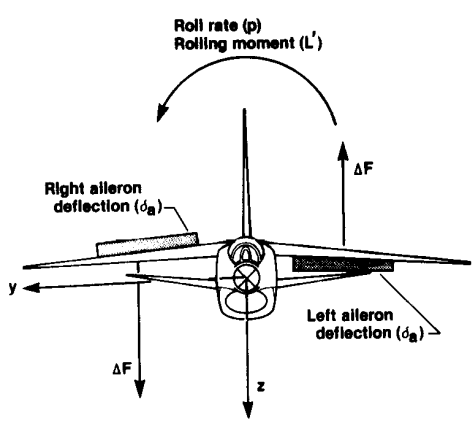

Fig. 5 Simplified aircraft nomenclature.

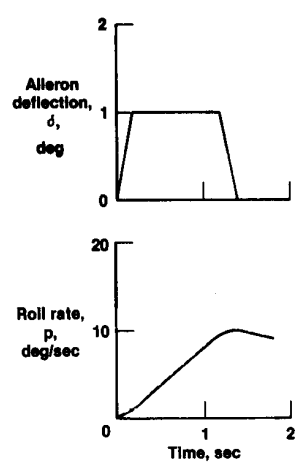

Fig. 6 Time history with no measurement noise.

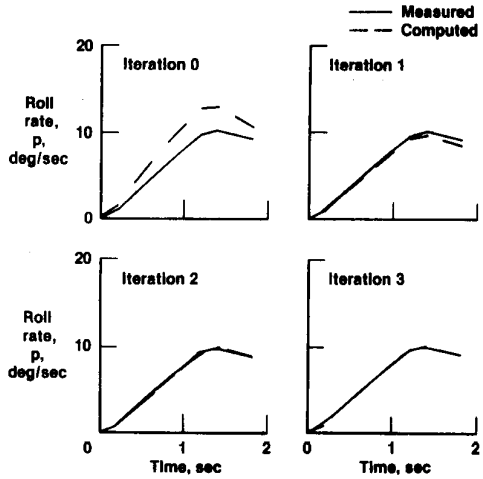

Fig. 7 Comparison of measured and computed data for each of the first three iterations.

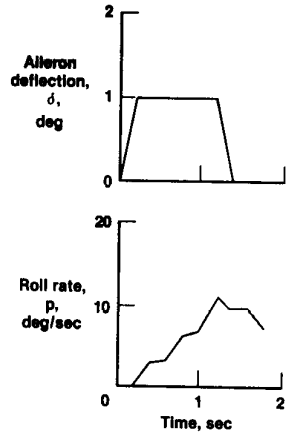

Fig. 8 Time history with measurement noise.

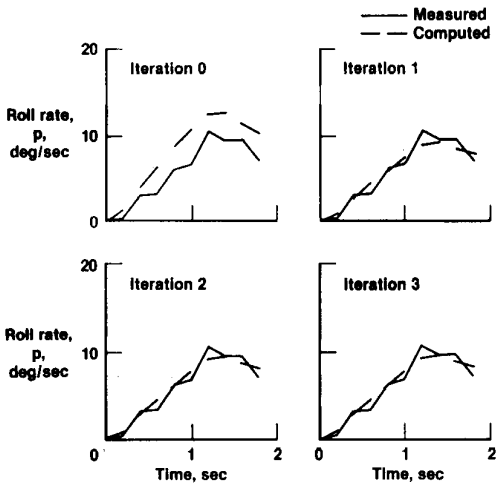

Fig. 9 Comparison of measured and computed data for each iteration.

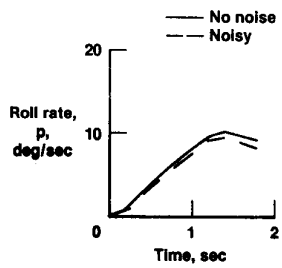

Fig. 10 Comparison of estimated roll rate from no-noise and noisy cases.

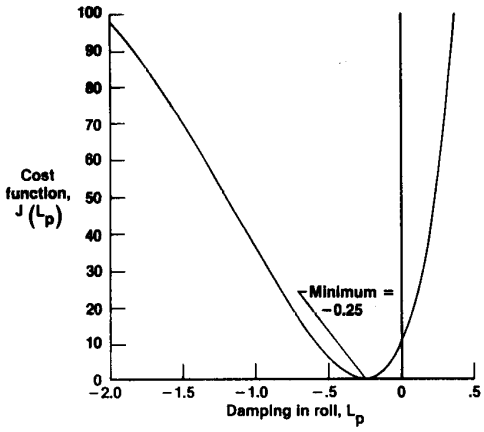

Fig. 11 Cost function ($J(L_p)$) as a function of L_p for no-noise case.

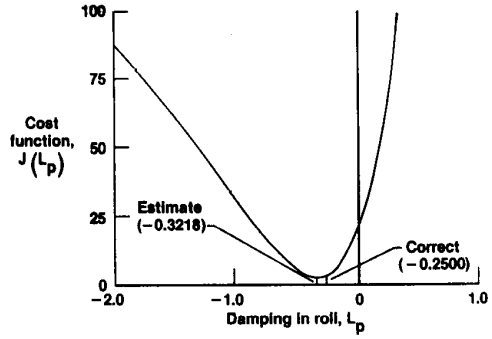

Fig. 12 Cost function as a function of L_p for noisy case.

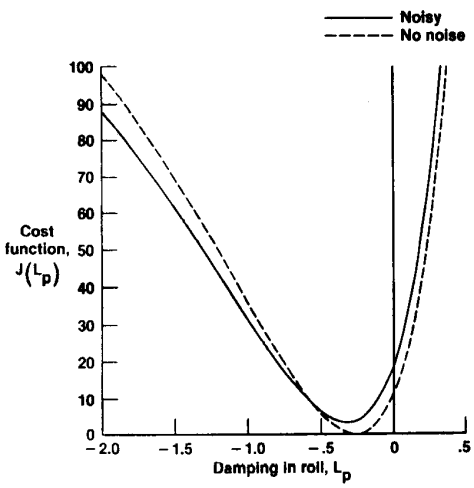

Fig. 13 Comparison of the cost functions for the no-noise and noisy cases.

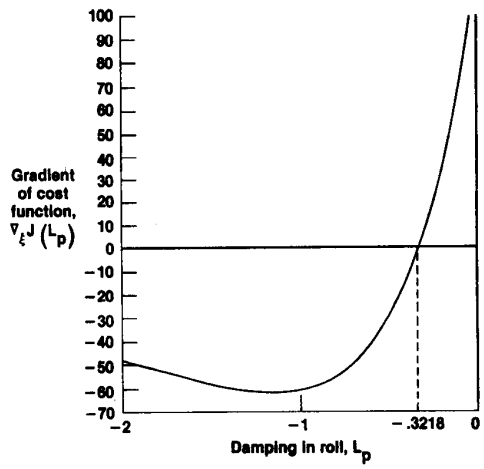

Fig. 14 Gradient of $J(L_p)$ as a function of L_p for noisy case.

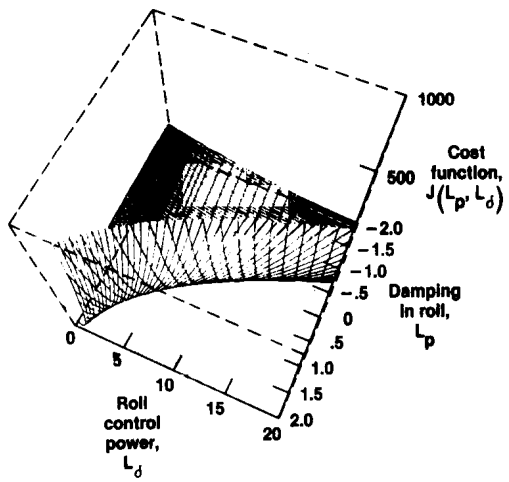

Fig. 15 Large-scale view of cost function surface.

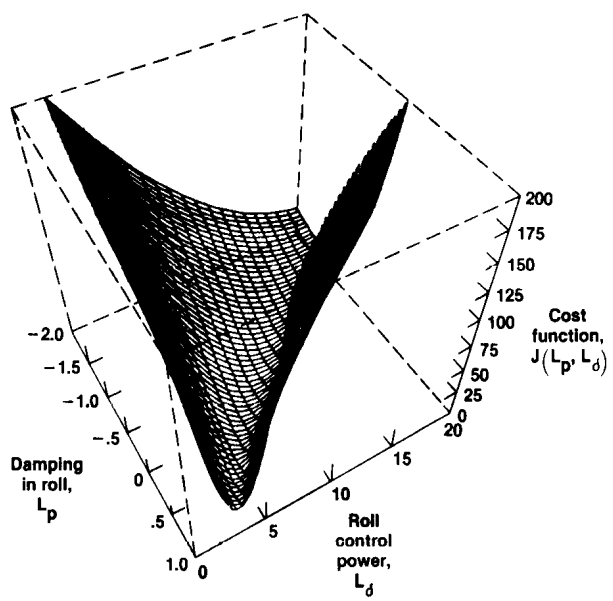

Fig. 16 Restricted view of cost function surface.

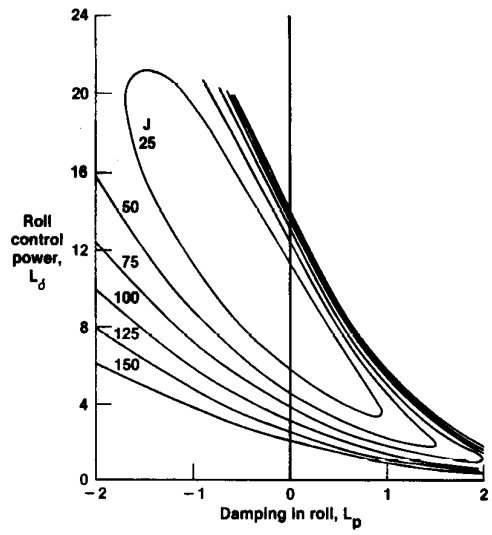

Fig. 17 Isoclines of constant cost of L_p and L_δ for the no-noise case.

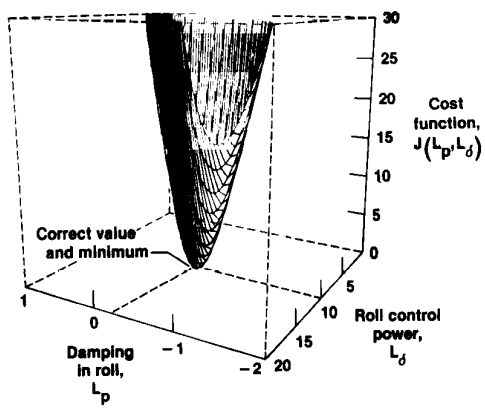

Fig. 18 Detailed view of cost function surface for no-noise case.

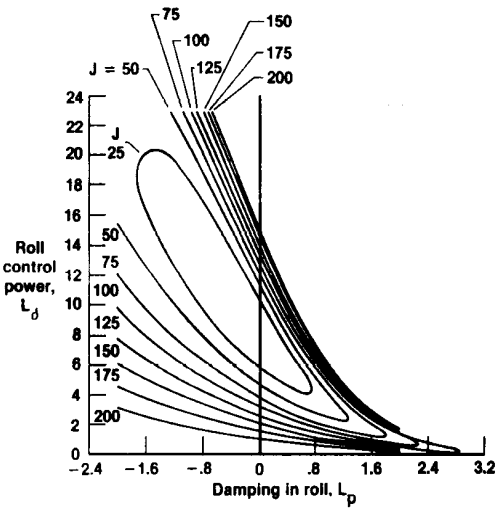

Fig. 19 Isoclines of constant cost in L_p and L_δ for the noisy case.

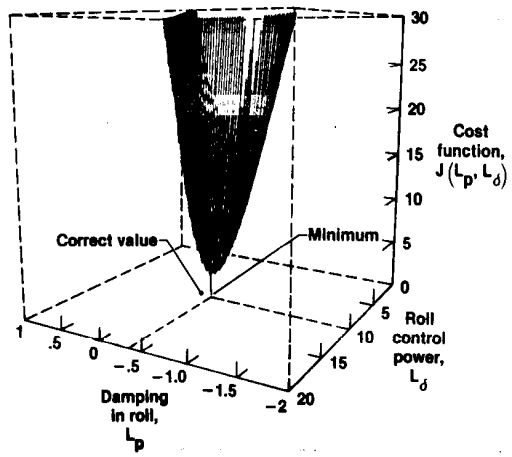

Fig. 20 Detailed view of cost function surface for noisy case.10

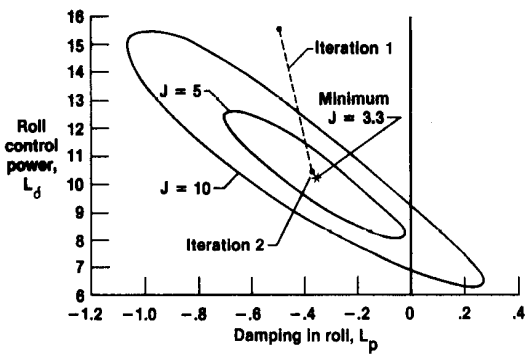

Fig. 21 Isoclines of constant cost for region near minimum for noisy case.

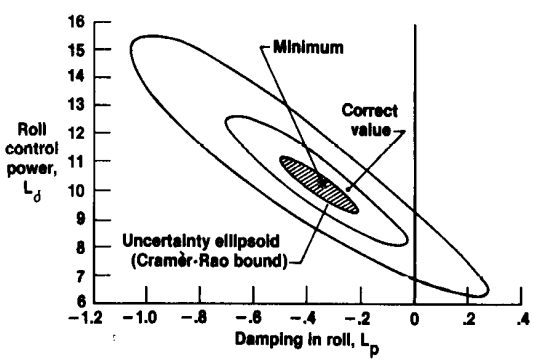

Fig. 22 Isoclines and uncertainty ellipsoid of the cost function for the noisy case.

1. Report No.	2. Government Accession No.	3. Recipient's Catalog No.
NASA TM-86730		

4. Title and Subtitle	5. Report Date
EXTRACTION OF AERODYNAMIC PARAMETERS FOR AIRCRAFT AT EXTREME FLIGHT CONDITIONS	May 1985
	6. Performing Organization Code
7. Author(s)	8. Performing Organization Report No.
Kenneth W. Iliff	H-1290
	10. Work Unit No.
9. Performing Organization Name and Address	
NASA Ames Research Center Dryden Flight Research Facility P.O. Box 273 Edwards, California	11. Contract or Grant No.
	13. Type of Report and Period Covered
12. Sponsoring Agency Name and Address	Technical Memorandum
National Aeronautics and Space Administration Washington, D.C. 20546	14. Sponsoring Agency Code
	RTOP 505-43-11

15. Supplementary Notes

Prepared as AGARD Paper 24, an invited paper for the AGARD Symposium on Unsteady Aerodynamics — Fundamentals and Applications to Aircraft Dynamics, Göttingen, Federal Republic of Germany, May 6-9, 1985.

16. Abstract

The maximum likelihood estimator has been used to extract stability and control derivatives from flight data for many years. Most of the literature on aircraft estimation concentrates on new developments and applications, assuming familiarity with basic concepts. This paper briefly discusses the maximum likelihood estimator and the aircraft equations of motion that the estimator uses. The current strength and limitations associated with obtaining flight-determined aerodynamic coefficients in extreme flight conditions is assessed. The importance of the careful combining of wind tunnel results (or calculations) and flight results and the thorough evaluation of the mathematical model is emphasized. The basic concepts of minimization and estimation are examined for a simple computed aircraft example, and the cost functions that are to be minimized during estimation are defined and discussed. Graphic representations of the cost functions are given to help illustrate the minimization process. Finally, the basic concepts are generalized, and estimation of stability and control derivatives from flight data is discussed.

17. Key Words (Suggested by Author(s))	18. Distribution Statement
System identification; Parameter estimation; Maximum likelihood; Cost functions; Stability and control; Extreme flight conditions	Unclassified-Unlimited STAR category 66

19. Security Classif. (of this report)	20. Security Classif. (of this page)	21. No. of Pages	22. Price*
Unclassified	Unclassified	22	A02

For sale by the National Technical Information Service, Springfield, Virginia 22161.